Assessment and ANN model development of natural light transmittance of light-transmitting concrete

Shing Mei Chiew [a], Izni Syahrizal Ibrahim [a, *], Mohd Azreen Mohd Ariffin [a], Han-Seung Lee [b], Jitendra Kumar Singh [c, d]

[a] *Forensic Engineering Centre (FEC), Institute for Smart Infrastructure and Innovative Construction (ISIIC), Faculty of Civil Engineering, Universiti Teknologi Malaysia, 81310, Johor Bahru, Johor, Malaysia*
[b] *Department of Architectural Engineering, Hanyang University, 1271 Sa3-dong, Sangnok-gu, Ansan, 15588, South Korea*
[c] *Innovative Durable Building and Infrastructure Research Center, Center for Creative Convergence Education, Hanyang University, 1271Sa3-dong, Sangnok-gu, Ansan, 15588, South Korea*
[d] *Department of Chemistry, Graphic Era Deemed to Be University, Bell Road, Clement Town, Dehradun, Uttarakhand, 248002, India*

ARTICLE INFO

ABSTRACT

This study aims to reveal the potential of Light-transmitting concrete (LTC) in transmitting natural light or sunlight, and to investigate the relationship between fibre diameter, fibre spacing, solar incidence angle, surface area, and light transmittance properties. The artificial neural network model as well as explicit equations from the model were developed to predict the light transmittance of LTC. The surface area was altered by varying LTC block arrangements from one to six. It was found that light incidence angle significantly affected the light transmittance of LTC. The highest light transmittance of LTC was achieved near solar noon, but it decreased drastically as soon as the solar incidence angle exceeded the acceptance angle. The effect of the LTC surface area and solar incidence angle on light transmittance diminished with a smaller fibre diameter or larger fibre spacing. The ANN model and explicit equations developed from the network provide good accuracy in predicting light transmittance of LTC.

1. Introduction

Light-transmitting concrete (LTC) is an innovative concrete that has emerged in recent decades. It allows light to pass through optical fibres embedded in opaque concrete. LTC not only adds to its aesthetic value, but is also capable of significantly reducing energy consumption [1,2] by allowing natural light into buildings, thus improving indoor daylighting. It has been proven that sunlight, which is a sustainable light source instead of artificial lighting, provides a more pleasant ambience and healthier workplace, directly improving work productivity [2]. LTC can be made with different types of translucent materials, namely optical fibre, waste glass aggregates, epoxy resin, plastic rods and many others. Among all the translucent elements, optical fibres are the most commonly used for LTC fabrication due to their excellent light transmittance properties which they transmit light through total internal reflection [3].

In general, previous researchers have found that the larger the fibre diameter, the higher the light transmittance of LTC [4–6]. However, Mosalam and Casquero [7] found that for the same fibre volumetric fraction, LTC with optical fibres of smaller diameter had higher light transmittance. This is because LTC tends to include a higher amount of optical fibre with smaller diameter and therefore, they are more densely arranged than those with larger fibre diameters under the same volumetric fraction. This statement is also consistent with the study by Shitote et al. [8]. On the other hand, fibre spacing was less commonly considered by previous researchers as compared with fibre volumetric fraction and fibre diameter [9]. In general, smaller fibre spacing leads to higher light transmittance of LTC. Huang [10] concluded that fibre spacing, fibre diameter, and fibre volumetric fraction are correlated and that the changes of these factors leads to different light transmittance properties of concrete. Altlomate et al. [5] found that smaller fibre spacing or higher fibre volumetric fraction were not always beneficial for the light transmittance of LTC, as in some cases, larger fibre diameter and fibre spacing resulted in higher light transmittance. This could be due to the combined effect of fibre diameter and fibre spacing on the light transmittance of LTC, regardless of the fibre volumetric fraction.

It is worth noting that most of the previous studies were experimental works in which the light transmittance tests were carried out indoors with artificial light as the light source. This only revealed the light transmittance properties of LTC under artificial light, but the properties may not be the same when tested under natural light, as the light intensity of sunlight is much higher than artificial light. Additionally, the position of sunlight varies throughout the day. Therefore, in order to investigate the light transmittance properties of LTC and its potential to reduce light energy consumption, it is necessary to conduct experimental work using natural light as the light source.

There are only a few studies that have conducted light transmittance tests under natural light or sunlight. Mosalam and Casquero [7] used perforated wood incorporating optical fibres and acrylic rods to represent the LTC panels, and tested under direct sunlight. They investigated several factors that affect the light transmittance properties of LTC, including the fibre volumetric fraction of the embedded fibres, fibre grid, fibre spacing, panel thickness, and the presence of concentrated parabolic compounds (CPCs). They concluded that LTC panels with smaller fibre diameter, where the fibre volumetric fraction was kept constant, had higher light transmittance, especially at noon. In contrast, also at noon, the light transmittance of panels with larger fibre diameters decreased because the fibres which were close to the corner of the panels had the transmitted light striking the black inner wall of the testing board, which was unable to be measured by the lux meter.

Tahwia et al. [11] performed light transmittance tests under sunlight on LTC specimens from 7.00 a.m. to 7.00 p.m., with fibre diameters of 1.0 mm and 2.0 mm, and with different fibre volumetric fractions (1%, 2%, 3% and 4%). They concluded that the relationships from the data of light transmittance of LTC throughout the day were similar to a Gaussian bell-shaped curve, where the maximum light transmittance was achieved at 1.00 p.m. They also reported that the fibre volumetric fraction affected the light transmittance of LTC more significantly than the fibre diameter, which was probably due to the convergence of the fibre diameters arranged in the fibre bundles. Similar tests on light transmittance were carried out by the same authors [12], but with high performance translucent concrete, which also gave similar results.

On the other hand, Su et al. [2] developed a simulation model using ray-tracing method to determine the daylighting performance of LTC considering the fibre volumetric fraction, fibre numerical aperture, light incidence angle of the sun, and latitude of the test site. They found that the light intensity decreased sharply when the incident angle of the sunlight exceeded the acceptance angle of the optical fibres. The larger numerical aperture of the fibres allowed for a longer daylight period with a more stable illuminance level. However, a larger numerical aperture of the fibres carried the risk of excessive daylight illumination, which was undesirable. In another study by the same authors [13], the optical and thermal impact of LTC were investigated considering the same factors, but with a full-scale south-facing LTC wall. It was found that both the optical and thermal transmittance of the LTC wall depended on the climate, as it could achieve high transmittance in winter, while low transmittance in summer. This reduced the daily heat loss and increased the daily heat gain in winter, although the installation of optical fibre worsened the thermal insulation of the wall.

Lian and Yin [14] conducted simulations to analyse the lighting situation in a building with the implementation of LTC concrete blocks. They found that the implementation of LTC increased the illuminance level by 24% in both the ground floor bedroom and living room, 9% in the dining room, and 80% in the kitchen.

Several studies [1,15–17] have also conducted simulations on LTC, but mostly concentrating on the reduction of energy consumption and energy conservation in terms of daylighting performance, and heating and cooling loads required due to thermal conduction of LTC walls. To the best of the author's knowledge, translucent materials used in buildings, such as windows, take into account the window-to-floor ratio to achieve the desired daylighting. Excessive daylight from a large window-to-floor ratio is undesirable as it can cause glare and visual discomfort. However, too little daylight is insufficient for a healthy working environment and productivity.

Similar to windows, the effect of LTC illuminance area on light transmittance appears to be important in determining the effective illuminance of a building. However, it is impossible for the LTC wall panel to have a variation of parameters; for example, volumetric fraction of fibres (different fibre-to-concrete area ratio), which is uneconomical and impractical. Therefore, it is necessary to investigate the effect of surface area (with fixed fibre parameters) by changing the number of LTC blocks on the light transmittance properties. This will provide researchers and Engineers insight into the extent to which the improvement of light transmittance through the variation of the surface area is possible in the design of LTC wall panels. Apart from the aforementioned parameters, experiments conducted by Sawant et al. [18] are the only ones that considered the effect of different surface areas of LTC on light transmittance under sunlight, but the analysis on the effect of surface area of LTC on light transmittance was limited.

Apart from the simulation models mentioned, it is also necessary to develop a computational method or model to estimate the light transmittance of LTC and to determine the relationships and significance of the parameters on the light transmittance. One of the computational methods that has emerged in recent decades is artificial neural networks (ANN), which can model complex relationships between the parameters and the output data without compromising accuracy [19,20]. This can reduce tedious and time-consuming experimental works. The architecture of ANNs consists of an input layer, hidden layer(s), neurons, transfer function, learning algorithm, and output layer(s), of which the data can be fed into the network, learnt, and trained by the neurons in the hidden layer(s), after which, the desired output for estimation can be achieved [21]. Mohandes et al. [22] stated that estimation is favourable in ANNs because of their fast processing time, short development, reliable prediction, and the ability to overcome the non-linearity between the inputs and the outputs.

ANN application has gained attention in Civil Engineering in recent decades due to the existence of a large number of complicated problems which are hard to analyse through traditional complicated calculations [23]. Moradi et al. [19] compared the predictions of concrete compressive strength containing metakaolin using empirical approach and ANN. They found that ANN showed excellent accuracy in predicting the concrete compressive strength with an error range of within $\pm20\%$ as compared with the empirical equation, where 68% of the predictions were within the $\pm40\%$ error range. Ramkumar et al. [24] analysed the performance of steel fibre self-compacting concrete using ANN and found that the developed models have the potential to replace the existing conventional regression model with a predictive reliability of 0.9995.

Gupta et al. [25] used ANN to predict the mechanical properties of rubberised concrete exposed to elevated temperatures, and determined the contribution of the input parameters to output parameters using the explicit equations generated from the study. They found out that the variation of exposed temperatures had the highest impact on all the output parameters, including compressive strength and Modulus of Elasticity, compared to rubber fibre content, water-to-cement ratio, and duration of exposure. Chithra et al. [26] conducted a comparative study using regression analysis and ANN to predict the compressive strength of high performance concrete (HPC) containing nano silica and copper slag. They stated that in situations that demand higher accuracy and involve high complexity, ANN provides better results with higher accuracy in the prediction of compressive strength as compared to regression models, which seemed inadequate with low coefficient of determination. Congro et al. [27] compared five different ANN architectures which involved different numbers of neurons in predicting the residual flexural strength of fibre reinforced concrete. They used the hyperbolic tangent sigmoid transfer function (*tansig*) and Bayesian regularization algorithm in their network models. They found out that 36 neurons were the most suitable for the network to predict the residual

flexural strength with absolute error values for experimental data of less than 1 N/mm².

In summary, most of the previous studies used artificial light as the light source in their experimental works. Artificial light cannot fully represent the light spectrum of natural light. There is also a lack of investigation between the parametric relationship of fibre diameter, fibre spacing, LTC surface area, incidence angle of sunlight, and light transmittance properties of LTC. Therefore, the fabrication of LTC in this study using SCC is aimed to reveal its potential to transmit natural light during daytime, and to investigate the relationship between fibre diameter (0.75 mm, 1.0 mm, 1.5 mm, and 2.0 mm), fibre spacing (15 mm, 18.75 mm, and 25 mm), solar incidence angle, number of LTC blocks (one to six blocks for varying surface areas), and light transmittance properties under sunlight. Besides that, this study also aims to develop an ANN model using backpropagation algorithm, considering the parameters in the experiments, to predict the light transmittance of LTC.

2. Materials and methods

2.1. Materials and concrete mix

Polymethylmethacrylate (PMMA) optical fibres were used in this study to fabricate LTC due to their excellent light transmittance properties [3]. Besides that, PMMA optical fibres are low cost and have high chemical resistance [9,28], and it is assumed that the heat produced during the cement hydration does not have an adverse effect on its chemical composition or light transmittance properties. Table 1 shows the physical properties of PMMA optical fibres.

Self-compacting concrete (SCC) was used to cast LTC in order to minimise the hindrance of concrete flowing through the closely arranged optical fibres, and to reduce the possible occurrence of voids and honey combs. Previous studies fabricated their LTC without coarse aggregates so that a maximum number of optical fibres can be embedded to achieve better light transmittance performance [5,29–31]. However, besides its aesthetic purposes, LTC also has the potential to be used as a structural material, for instance, as load-bearing walls, and as such, the elimination of coarse aggregates is impossible. Therefore, in this study, coarse aggregates were included in the concrete mix for the production of LTC.

Table 2 shows the self-compacting concrete mix design in reference to the study by Siddique [32]. Ordinary Portland cement (OPC) or CEM I type was used with 65% of carbon oxide (CaO), 21% of silicon oxide (SiO₂), and 6% of aluminium oxide (Al₃O₂). Class F fly ash with a dosage of 30% by weight was used as part of its cement replacement. This was based on the recommendation from previous studies [32–34] where they concluded that 30% was the optimum dosage for fly ash in terms of both fresh concrete properties and mechanical properties. Fly ash was used in the SCC mix to enhance the concrete flowability [35], which is required for the passing ability through the optical fibre during concrete placement without any compaction. The composition of Class F fly ash is shown in Table 3. Sand as fine aggregate was used in the concrete mixture with a passing percentage of 54.4% through the 600 μm sieve, while the maximum particle size of the crushed coarse aggregate was 10 mm. The superplasticiser used in this study was polycarboxylic ether-based Type F admixture complied with ASTM C494 and BS-EN

Table 1
Properties of PMMA optical fibre.

Core Material	*Polymethylmethacrylate*
Cladding Material	Fluorinated polymer
Working Temperature	−50 °C–70 °C
Attenuation Loss	≤250 db/km
Numerical aperture	0.51
Acceptance angle	30.66°

Table 2
Mix proportions of SCC for 1 m³ in reference to the mix design by Siddique [32].

Cement (kg/m³)	385
Fly Ash (kg/m³)	165
Fine Aggregate (kg/m³)	590
Coarse Aggregate (kg/m³)	910
Water (kg/m³)	253
Superplasticiser (L/100 kg Cementitious Material)	0.5

Table 3
Chemical composition of Class F fly ash.

Composition	Content (%)
Al₂O₃	21.3
SiO₂	59.5
SO₃	0.6
Fe₂O₃	7.1
CaO	7.18
MgO	1.42
K₂O	1.53
Na₂O	1.42

934–2:2012 [36]. The superplasticiser is milkfish in colour, and provides high workability and excellent concrete quality during casting [37].

2.2. LTC fabrication

The formwork was prepared using wooden boards with holes drilled into them to allow the optical fibres to pass through. The minimum spacing between the holes was kept at 15 mm, so that the 10 mm coarse aggregates can pass through between the optical fibres without obstructing the casting work. The holes were drilled with fibre arrangements of 4 × 4 grids (25 mm fibre spacing), 5 × 5 grids (18.75 mm fibre spacing), and 6 × 6 grids (15 mm fibre spacing) as shown in Fig. 1. The optical fibres were manually inserted into the predrilled holes before assembling the formwork.

A total of 36 LTC cube blocks with dimensions 100 mm wide × 100 mm high × 100 mm long were cast according to *The European Guidelines for Self-Compacting Concrete* [38]. The design strength of the concrete was 40 N/mm² 18 specimens were cast with constant fibre diameter of 2.0 mm but different fibre spacing, while another 18 specimens were cast with constant fibre spacing of 15 mm but with different fibre diameters. Upon the completion of the concrete mixing, the fresh concrete property tests of the SCC, e.g., slump flow test, V-funnel test, and L-box test, were carried out before placing them in the formwork to ensure that the concrete mix achieved the desired flowability, filling ability, and passing ability, respectively, according to the European Guidelines. After the fresh properties' tests, the concrete was allowed to flow freely into the formwork without a compaction process. The cast specimens were cured for 24 h at room temperature and 28 days in the curing tank before testing. The plain SCC was tested at 28 days in accordance with BS EN 12390–3:2009 [39] to determine the compressive strength with the loading direction perpendicular to the direction of the optical fibre arrangement.

2.3. Light transmittance test setup

A lux meter was used to measure the light intensity transmitted by the LTC blocks under sunlight, because it directly measures the light intensity in lux, which is the unit of illuminance in the International System of Units (SI). The light transmittance field test was conducted with the test setup facing south at the walkway of Structure and Material Laboratory, Universiti Teknologi Malaysia. The light transmittance testing board was designed as shown in Fig. 2. The openings made at the top of the wooden board were to allow the placement of the LTC blocks,
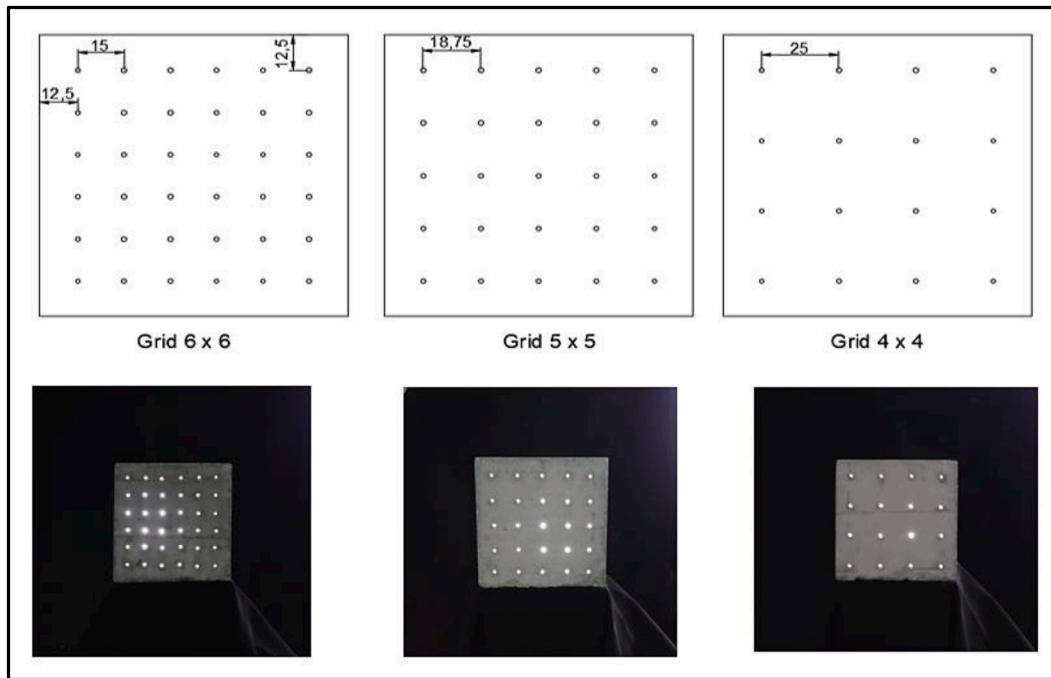
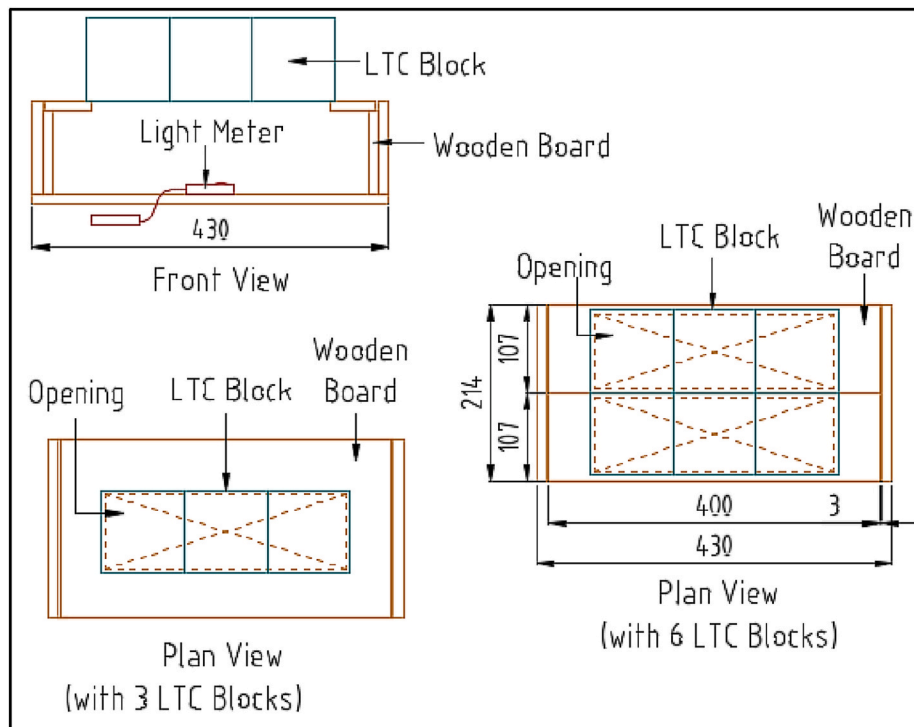**Fig. 1.** Fibre arrangement of LTC specimen.

Fig. 2. Light transmittance test setup with different number of LTC specimen that altered the LTC surface area.

while at the same time allowing light to pass through so that it can be measured by the lux meter. The lux meter was placed at the bottom-centre of the wooden board. The inner surface of the wooden board was painted black to minimise light reflection and to ensure that all transmitted light detected by the lux meter came directly from the LTC blocks. In order to measure the light transmittance of LTC with varying surface areas, wooden boards with two types of openings were fabricated to allow the measurement of light transmittance from one to six blocks, as shown in Fig. 2. The arrangement of LTC blocks for varying

the surface area is shown in Fig. 3.

The light transmittance test was carried out from 9.00 a.m. to 4.00 p. m. because the light intensity of LTC before 9.00 a.m. and after 4.00 p.m. is insignificant due to low initial light intensity and the large solar incidence angle. The chosen weather for the testing was either clear blue sky (<30% of cloud cover) or intermediate sky (30%–70% of cloud cover) [40] because the initial measured light intensity showed no significant difference between these two types of day sky, as detected by the lux meter. Five measurements were taken consecutively every hour
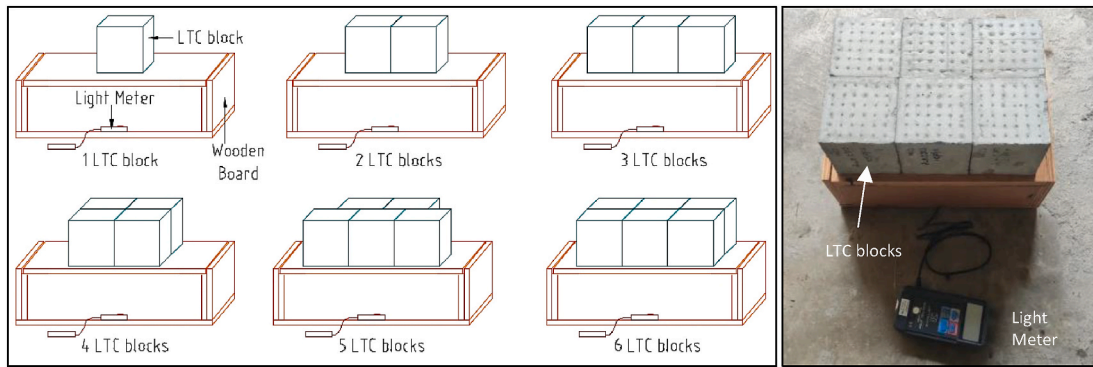
Fig. 3. LTC block arrangement for light transmittance test under sunlight.

from 9.00 a.m. to 4.00 p.m. for each LTC blocks arrangement of one to six. Averages of the measurements of every hour were then taken. The test was discontinued when the sky became dark or if it started to rain. The result data were only considered for further analysis if continuous measurements were taken throughout the period time from 9.00 a.m. to 4.00 p.m. on the field test.

Solar incidence angle (θ_i) is referred to as the angle between the normal to the plane surface of the specimen and the direction of the sunlight. The term θ_i can be computed using Eq. (1) as follows:

$$\theta_i = 90° - \theta_a, \text{ at horizontal plane} \tag{1}$$

where θ_a is the solar altitude angle, of which the angle is between the sun's ray and the surface of the horizontal plane. The solar altitude angle was obtained using the Solar Elevation Angle Calculator [41]. To investigate the light transmittance of the LTC, light transmittance in unit lux and in percentage (ρ) using Eq. (2) was considered:

$$\rho = \frac{L_T}{L_0} \times 100\% \tag{2}$$

where L_T is the light transmittance through LTC in lux, and L_0 is the initial light intensity in lux.

3. ANN model development

Artificial neural network (ANN) is a computational model which simulates the biological neural network of human brain to process information and data through neurons. When data is fed into ANN, the network learns and adjusts the weights and biases in the hidden layer(s) until a desirable output is obtained. It is proven to have the tendency to cope with non-linearity, determine the relationship between the input and output variables, adapt changes through learning, and has high fault tolerance [26]. MATLAB mathematical software (R2022b) was used to develop the ANN model in this study. Fig. 4 shows the flowchart of the methodology in developing the ANN model. After collecting the raw data from the experiments, they were pre-processed to make the training easier and more efficient. This pre-processing of data is to avoid any iteration from being stuck at the local minima which may generate undesirable results [21,42]. In this study, input variables including fibre diameter, fibre spacing, number of LTC blocks, light incidence angle, and initial light intensity were considered in the ANN model. Initial light intensity was recorded during the experimental works as a passive variable. Min-max transformation was used to pre-process the input data (x) so that the input variables have a standard range of [0,1], using the maximum and minimum values (x_{max} and x_{min}, respectively) of each
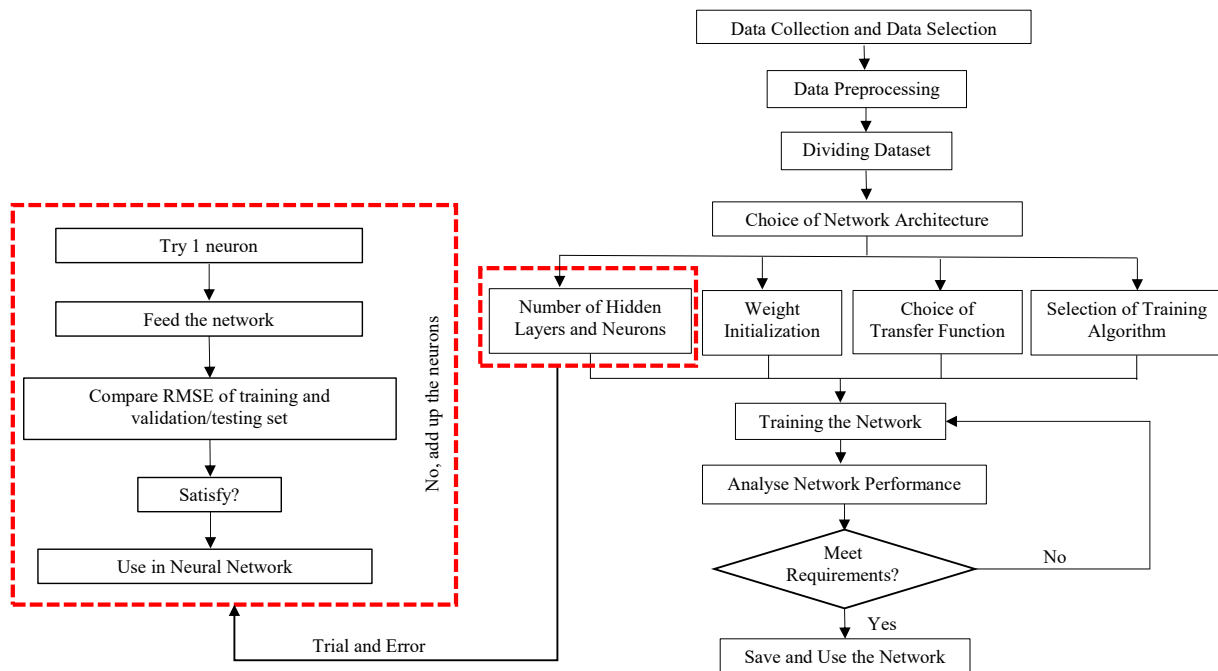

Fig. 4. Flowchart of methodology in developing ANN model.

variable, shown in Table 4 and Eq. (3), as follows:

$$x_n = (x - x_{min}) / (x_{max} - x_{min}) \tag{3}$$

For the output variable, which is light transmittance, the data points were first plotted in MATLAB to understand the data distribution. It was found that the data points tend to skew to the left, which is undesirable, as shown in Fig. 5(a). Hence, logarithmic transformation was used to transform the output data to reduce the potential of unequal variance residuals for data distribution of neuron activations between the network layers [43]. The output data (y) was transformed to be more normally distributed (shown in Fig. 5(b)) after applying the logarithmic function using Eq. (4):

$$y_n = \log(y + 1) \tag{4}$$

When building the network architecture, the number of neurons, choice of transfer function, and learning algorithm are decided. In this study, the *tansig* transfer function was used in the hidden layer of the ANN model because of its steeper output gradient of range $[-1, 1]$ which can detect small deviations in the input variables with a much stronger non-linear response [44]. The *tansig* transfer function can be expressed in Eq. (5) as follows:

$$tansig = \frac{2}{1 + e^{-2\left(\sum_i w_i x_i + w_0\right)}} - 1 \tag{5}$$

where i is the index of the input neuron, w is the weight of the neuron, x_i is the input of the neuron and w_0 is the bias to the neuron. For the output layer, *purelin* transfer function was used to fit the net output of the hidden layer to the target output.

For the learning algorithm, Bayesian regularization (BR) and Levenberg-Marquardt (LM) algorithms were considered, because both used Jacobian derivatives which perform faster than other algorithms that used gradient derivatives. After the performance comparison of both algorithms, the Bayesian regularization (BR) algorithm was used in the development of the ANN model to generate the explicit equations. Generally, the dataset is divided into a training dataset, validation dataset, and testing dataset. But since the BR algorithm is used, the validation dataset is not required as the algorithm has its own built-in validation process [45]. Therefore, the training set consisted of 85% of the dataset, whereas the testing set consisted of 15% of the dataset. There is no standard rule in deciding the suitable number of neurons in ANN. Most of the previous studies [19,25,45] used trial-and-error methods to determine the number of neurons to be used in the network. In this study, the network architecture consisted of one hidden layer and seven neurons which were determined through trial and error, with the smallest difference of the root mean square error (RMSE) between the training set and testing set.

4. Analysis of network and process of generating explicit equations

For the network analysis, the overall performance of the ANN model was presented as a correlation coefficient (R), which determined whether the predicted output from the model was well fitted to the

targeted output. The performance graphs with *R* values were presented for the training dataset, testing dataset, and the overall performance of the network for the BR algorithm. Besides the *R* value, mean square error (MSE), root mean square error (RMSE), epoch of the network, error histogram, and error range of the network were presented. In order to further validate the performance of the network, a blind test with new data which was never exposed to the network, was fed into the network. The blind test consisted of the results randomly selected from the data collected in the testing day where the tests were terminated due to poor weather conditions.

After achieving the satisfied network model, the trained ANN was saved and the weights and biases of the hidden layers were extracted from the model to develop the explicit equations. The output of the ANN model, O_s can be computed using Eq. (6) and Eq. (7) [25] as follows:

$$O_s = bias_s + \sum_{k=1}^{r} \left(\frac{2}{1 + e^{-2H_k}} - 1 \right) \times w_{k,l}^{ho} \tag{6}$$

where,

$$H_k = \sum_{j=1}^{q} w_{j,k}^{ih} \times I_j + bias_k \tag{7}$$

where q is the number of input variables; r is the number of hidden neurons; s is the number of output parameters; $bias_s$ and $bias_k$ are the biases for sth output neuron and kth hidden neuron (H_k); $w_{k,l}^{ho}$ is the set of weights connecting the output layer and hidden neurons, and $w_{j,k}^{ih}$ is the set of weights connecting the input variables to the hidden neurons [25].

However, O_s is not the final value for the output of ANN if using explicit Eq. (6) and Eq. (7). It is necessary to consider the data pre-processing and post-processing blocks which automatically run in the network object when data is fed into the network. In the ANN tool of MATLAB, the data feed into the network was pre-processed using the *mapminmax* function which normalises the data to the range of $[-1, 1]$ by default. The *mapminmax* function is defined in Eq. (8) as follows:

$$y = 2 \times \frac{(x_n - x_{nmin})}{(x_{nmax} - x_{nmin})} - 1 \tag{8}$$

where y is the normalised data before it is fed into the network, x_n, x_{nmax} and x_{nmin} are the input matrix, maximum, and minimum values of the input matrix after first normalisation, respectively. Hence x_{nmin} and x_{nmax} of the input variables are 0 and 1, respectively, after first normalisation using Eq. (3). After computing the output from explicit equations using weights and biases, the output has to undergo a post-processing function which is the inverse of the *mapminmax* function, and lastly the inverse of logarithmic function, to obtain the light transmittance in unit lux. Fig. 6 presents the summary of the process in generating the explicit equations from the trained network.

5. Results and discussion

The SCC cast achieved the desired fresh properties with slump flow between 600 mm and 710 mm, V- funnel time ranging between 2 s and 5 s, passing ratio above 0.9, in addition to no segregation being observed. The fresh properties of SCC were said to achieve the requirements stated in *The European Guidelines for Self-Compacting Concrete* [38]. The average compressive strength at 28 days for the three 100 mm cubic SCC specimens was 45.71 N/mm^2, whereas the compressive strength of all the LTC specimens were within the range of 41 N/mm^2 and 47 N/mm^2 as shown in Fig. 7, which was desirable and above the design strength.

The concrete compressive strength had increased with the inclusion of the optical fibre and with the increment of fibre diameter from 0.75 mm to 1.0 mm. However, when the fibre diameter was further increased from 1.0 mm to 1.5 mm and 2.0 mm, the compressive strength decreased. This is due to a larger surface area of fibre being in contact
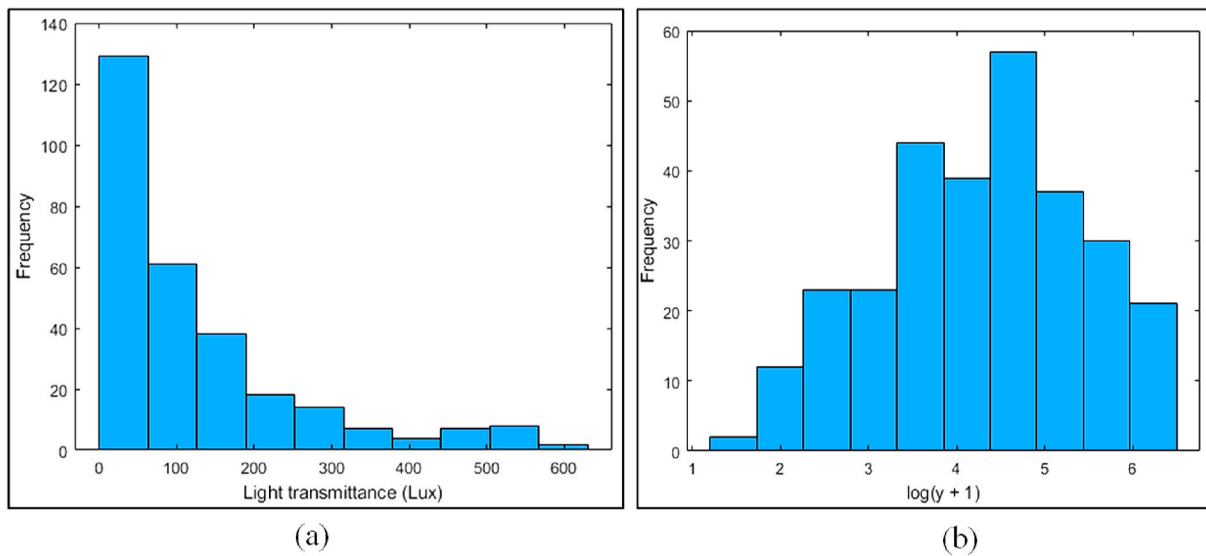
Table 4
Maximum and minimum values of respective input variables.

Parameters	Symbol	Values	
		Minimum, x_{min}	Maximum, x_{max}
Fibre Diameter	$\emptyset$	0.75	2
Fibre Spacing	S	15	25
No. Of Block	n	1	6
Light Incidence Angle	θ_i	0.62	59.69
Initial Light Intensity	L_0	9230	117,500

Fig. 5. Distribution of output data points: (a) before logarithmic transformation, and (b) after logarithmic transformation.

with the concrete matrix, in which the hydrophobic and smooth nature of the fibre surface results in the weak bond between the fibre-matrix interface. Besides that, the effect of fibre spacing on the 28-days compressive strength of concrete is found to be relatively insignificant compared to the fibre diameter.

Fig. 8 shows the light transmittance of LTC (ρ) under natural light to illustrate the proportion of light that passed through the LTC block(s). Fig. 8(a) shows the light transmittance of LTC with a constant fibre diameter of 2.0 mm, whereas Fig. 8(b) shows the light transmittance of LTC with constant fibre spacing of 15 mm. The blocks were classified with label 'LTC' followed by the fibre diameter as shown in Fig. 8. For instance, "LTC2.0″" indicates LTC block with a fibre diameter of 2.0 mm. The variation of each group is presented using different symbols and line types, whereas the variation of the surface area, which is determined by the number of LTC block arrangements, is presented using different colour tones.

In previous studies [7,11,18], the light transmittance of LTC under natural light was usually illustrated with the hourly measured time on the *x*-axis. Although the light transmittance changed with time, this was not sufficient to explain the relationship between the light transmittance of LTC and solar incidence angle. Therefore, in Fig. 8, instead of using the hourly measured time, the solar incidence angle was plotted on the *x*-axis, with the positive angle representing the solar incidence angle before solar noon (the highest position of the sun during the day occurred between 12.50 p.m. and 1.10 p.m. during the field test period), while the negative angle representing the solar incidence angle after solar noon.

The graphs shown in Fig. 8 are consistent with the graphs from the findings of the previous studies [2,7,11,12,18] in which the data points formed a Gaussian bell-shaped curve. However, it is difficult to compare the results with the previous studies because the test conditions are different, such as the test location (the sun position varies depending on the longitude and latitude, as shown in Fig. 9), sky conditions, local weather, and season (as Malaysia is located near the equator with tropical weather which experiences hot and humid climates throughout the year), and the parameters considered in the tests, such as the specimen size, fibre volumetric fraction, the numerical aperture of the optical fibre, and others. From Fig. 8(a), it was clear that for a constant fibre diameter of 2.0 mm, the smaller the spacing, the better the light transmittance properties of LTC. This is because the closer spacing of the optical fibres allows more adjacent light rays to interfere and overlap, resulting in higher light intensity. Additionally, smaller spacing allowed more optical fibres to be incorporated into the LTC blocks, which

directly increased the fibre content.

Furthermore, it is noteworthy that the light transmittance increased with the decreasing of solar incidence angle. When the solar incidence angle was within the acceptance angle range ($\pm 30.66°$, between 10.00 a. m. and 3.00 p.m.), the light transmittance increased dramatically as more light rays entered the optical fibres and underwent total internal reflection. All LTCs achieved the highest light transmittance between 12.00 noon and 1.00 p.m., when the light incidence angle was close to zero, regardless of the fibre diameter, fibre spacing, or number of LTC blocks arrangement. This is because the sun was almost perpendicular to the surface of the LTC blocks when the angle of light incidence was close to zero, allowing a maximum number of light rays to pass through the optical fibres by total internal reflection. However, after the solar noon, the solar incidence angle increased and eventually exceeded the acceptance angle of the optical fibre. More light rays were scattered and refracted out of the optical fibre instead of experiencing total internal reflection, thereby causing the light transmittance to decrease.

On the other hand, Fig. 8(b) shows that the light transmittance increased with the increase of the fibre diameter when the fibre spacing was kept constant at 15 mm. This is because a larger fibre diameter contributed to a higher ratio of fibre surface area to the concrete surface area, allowing more light rays to enter each optical fibre and undergo total internal reflection. This resulted in higher light transmittance. It is worth noting that the effect of the angle of solar incidence on the LTC was still significant at a fibre diameter of 2.0 mm, but as the fibre diameter reduced, the effect of solar incidence angle gradually diminished. This is particularly evident in the LTC blocks with a fibre diameter of 0.75 mm, where the light transmittance did not show any drastic or significant increase or decrease even though the solar incidence angle was within the acceptance angle. This is because only a limited number of light rays entered the smaller fibre diameter of the optical fibre as compared with the larger ones. Most of the light rays falling on the LTC specimens were either scattered, reflected from the concrete surface, or refracted out of the optical fibre.

It is noted that the surface area of LTC determined by the number of LTC blocks did not have significant effect on the light transmittance of LTC, as compared with fibre diameter, fibre spacing, and light incidence angle, as shown in Fig. 8. Nonetheless, the effect of the increment in the number of LTC blocks only became slightly significant when the fibre diameter increased to 2.0 mm, or the fibre spacing decreased to 15 mm (6 × 6 fibre grid). This can be explained by the fact that the increase of the LTC surface area by increasing the number of LTC blocks only amplified the original light transmittance properties of LTC. In other
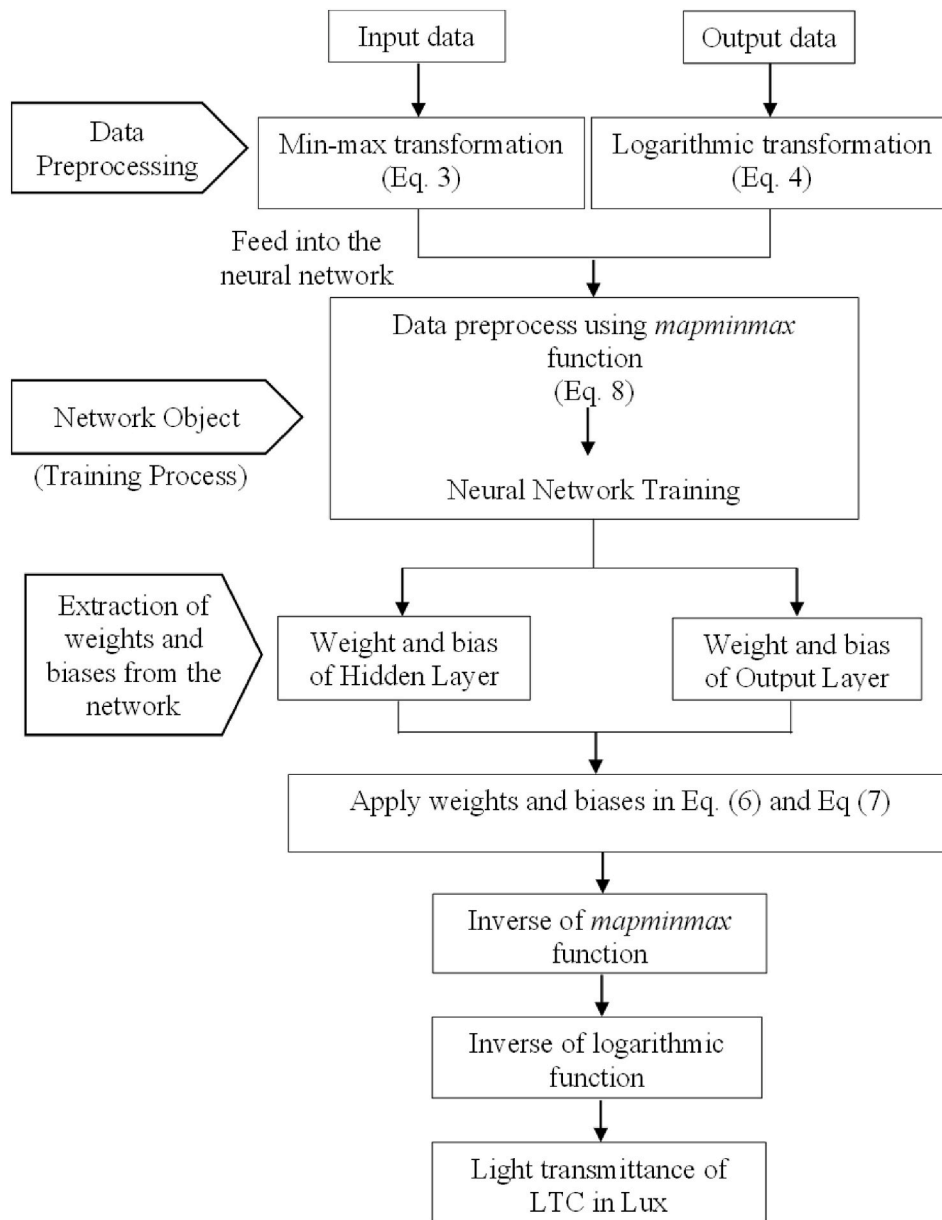
Fig. 6. Process of generating explicit equations from the trained ANN model.

words, if the fibre diameter is large (or with smaller fibre spacing), where the original light transmittance of one LTC blocks is higher, the amplification is large, or vice versa.

In order to have a clearer picture of the light transmittance properties when encountered with different solar incidence angles, the rate of increment or decrement of light transmittance was compared between LTC blocks with fibre diameters of 2.0 mm and 0.75 mm, and with the largest and smallest fibre spacing (15 mm and 25 mm), as shown in [Fig. 10]. The surface area for comparison was kept constant with a six blocks arrangement. The rate of increment and decrement was computed starting from 9.00 a.m. onwards. Therefore, it was assumed that the rate of change of light transmittance at 9.00 a.m. was zero. The last number of the legends in the figure represented the fibre spacing for comparison purposes. It was found that the rate of increase was the highest at 11.00 a.m. for LTC2.0 and LTC0.75. This is because the solar incidence angle between 10.00 a.m. and 11.00 a.m. was within the acceptance angle range of the optical fibres, which drastically increased the number of light rays entering the optical fibres and undergoing total internal reflection.

It is noteworthy that LTC0.75 had more drastic rate of increment as compared to LTC2.0. This could be due to the fact that fewer light rays entered the optical fibres for the 0.75 mm diameter than the 2.0 mm. This is attributed to the smaller relative surface area of the optical fibres with diameter of 0.75 mm to capture light rays when the solar incidence angle was beyond the acceptance angle. Hence, once the solar incidence angle was within the acceptance angle range, the difference in light transmittance of LTC0.75 at 11.00 a.m. as compared with the earlier hours was more significant than that of LTC2.0, even though the light transmittance of LTC0.75 was much lower.

Solar incidence angles were within the acceptance angle range between 11.00 a.m. and 2.00 p.m. It can be seen that the rate of increment for all the specimens decreased, regardless of the fibre spacing and fibre diameter. Among the compared specimens, LTC2.0 with a fibre spacing of 15 mm showed a drastic decrease in the rate of increment of light transmittance, and between 12.00 noon and 2.00 p.m., the rate of increment or decrement was very small and can be considered insignificant. This shows that further changes in the solar incidence angle within the acceptance angle range did not have much effect on the light
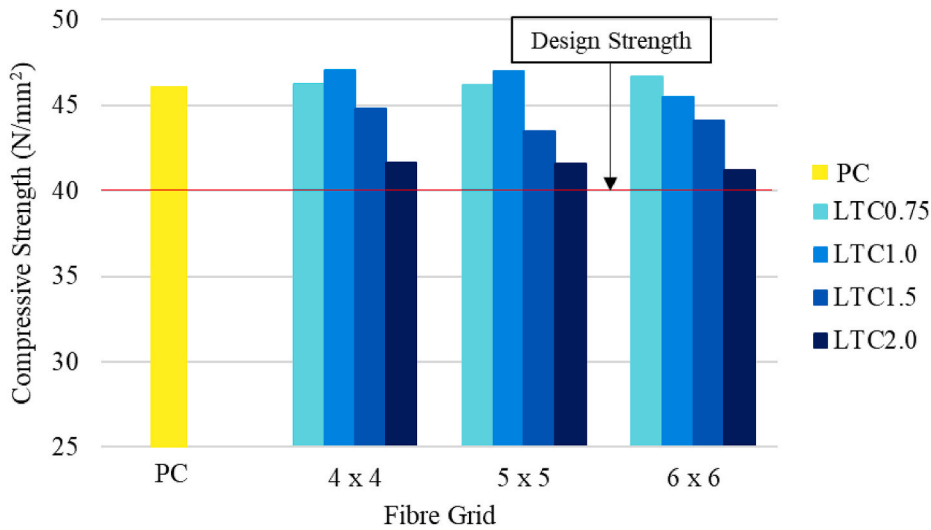
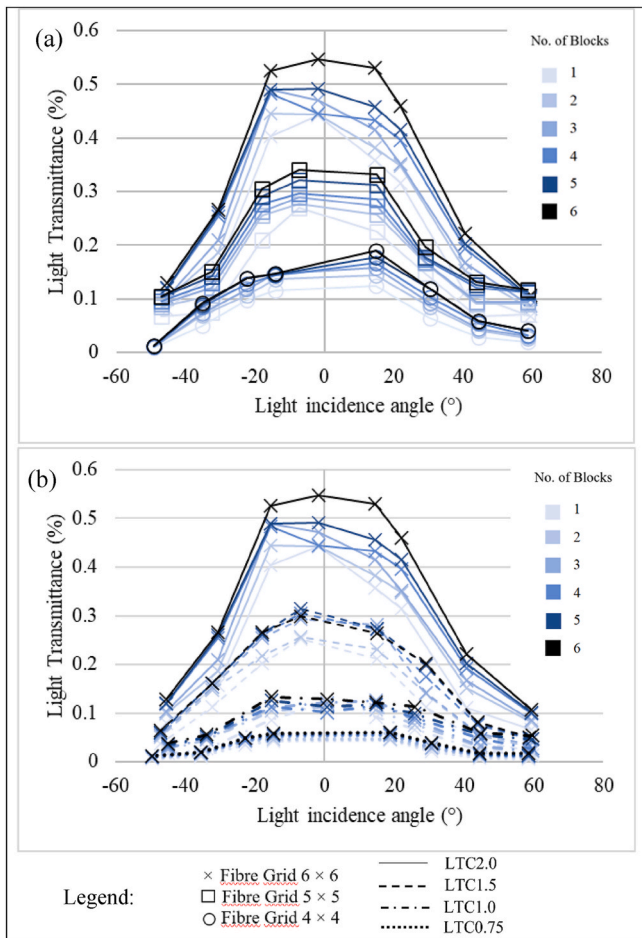Fig. 7. Compressive strength of control specimen and LTC specimens on 28 days.

Fig. 8. Light transmittance under natural light with (a) constant fibre diameter of 2.0 mm, and (b) constant 6 × 6 grids (fibre spacing of 15 mm)
*Notes: Number of block arrangement, LTC2.0: diameter (Ø) 2.0 mm; LTC1.5: Ø 1.5 mm; LTC1.0: Ø 1.0 mm; LTC 0.75: Ø 0.75 mm.

Fig. 9. Sun ray on earth [46].

transmittance of the LTC blocks. This indicates that LTC2.0 with a fibre spacing of 15 mm has the potential to maintain a slightly longer period of stable high illuminance as compared to LTC2.0 of 18.75 mm and 25 mm fibre spacing and LTC0.75 of 15 mm fibre spacing.
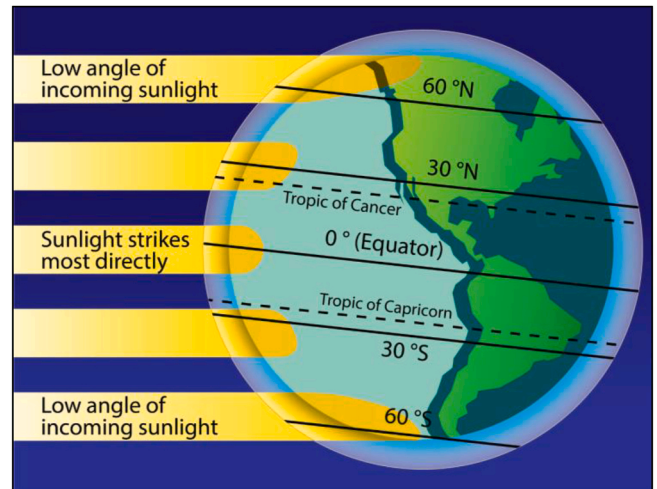
After 1.00 p.m. of which the time had passed the solar noon, the rate of decrement in light transmittance began to increase. This is because the solar incidence angle started to increase again after the solar noon. More and more light rays were reflected or refracted out of the core of the optical fibre instead of experiencing total internal reflection, resulting in a decrease in light transmittance. It is evident that there was a dramatic increase in the rate of decrement in light transmittance angle after 2.00 p.m. because the solar incidence angle had increased beyond the acceptance angle. The rate of decrement in the afternoon was not as high as the rate of increment of light transmittance in the morning. This is probably due to the fact that the intensity of sunlight in the afternoon decreased slower than the increment in the morning.

Based on the experimental results, LTC2.0 with fibre spacing of 15 mm performed the best in natural light transmittance, regardless of the number of blocks arrangement. According to MS 2680: 2017, the Malaysian Standard of on energy efficiency for residential building [40], the recommended range for useful daylight illuminance is 100 lux–2000 lux. In the experiment, only LTC2.0 with fibre spacing of 15 mm was able to transmit sunlight at more than 100 lux from 10.00 a.m. to 3.00 p. m., which is sufficient for residential buildings as recommended in the standard. Furthermore, it is undeniable that it is impractical to replace all windows in a building with LTC [13], but implementing LTC can definitely help to reduce light energy consumption without causing
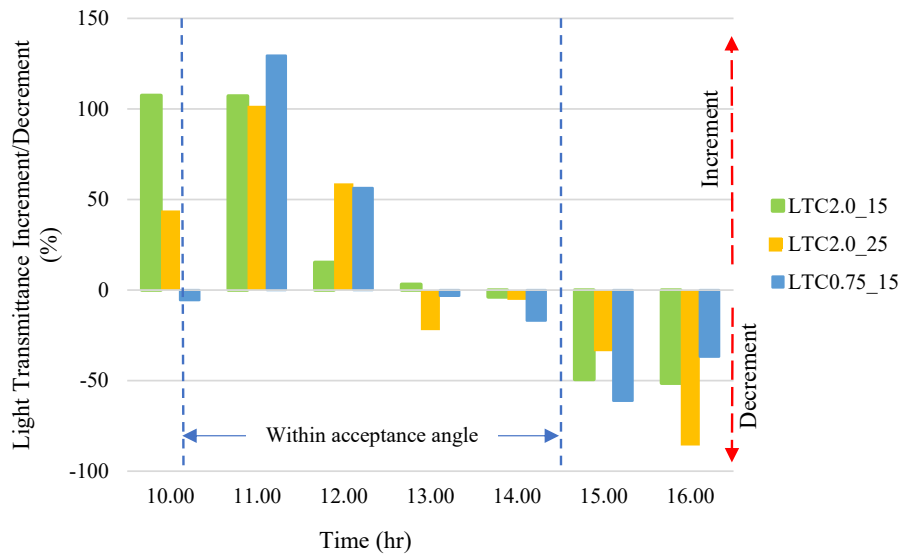
Fig. 10. Rate of increment or decrement of light transmittance throughout the day.

glare or visual discomfort.

6. Development of empirical approach to determine light transmittance of LTC

6.1. Analysis of ANN network

Fig. 11 presents the best training performance of the ANN model using BR algorithm, whereas Table 5 shows the comparison of the statistical indicators for training set and test set. The minimum MSE that can be achieved before the training is terminated is 0.00618 after 132 iterations. Both MSE and RMSE shown in Table 5 indicate that the model works relatively well with the points of dataset and the deviation between the predicted output and targeted output is relatively small. Besides that, R-values for training, testing and all data are above 0.997, which is close to 1.0, as shown in Fig. 12. This indicates that the trained model is well fitted to the data points in both training and testing datasets, and no overfitting was observed.

Fig. 13 presents the error histogram of the ANN model using BR algorithm. The error of the neural network is distributed over 20 bins and

Table 5
Comparison of statistical indicators of training set and testing set.

Dataset	MSE (unscaled)	RMSE (unscaled)	R
Train Data	0.00616 (117.3127)	0.0785 (10.8311)	0.9982
Test Data	0.007921 (133.2131)	0.0890 (11.5418)	0.9969

ranges from −0.1968 to 0.2275. The zero-error line falls under the bin with an error value of 0.0042, where 34 training data points fall within this range. This indicates that the difference between the predicted and targeted value of the training points of these data are close to zero. Moreover, most of the errors of the overall dataset are less than ±0.1 with no outliers found, which indicates a very good accuracy of the trained ANN.

Fig. 14 further explains the distribution of the percentage of estimations in various error ranges. All the datasets fall within an error of ±30%, where the maximum error of the network is 25.1% which consists of only one data estimate. Furthermore, 51.7% of the data estimates have less than ±5% error, and 78% of the estimations are within the ±10% error range, which shows that the trained ANN has high accuracy in estimating the light transmittance of LTC using BR algorithm. Error ranges which fall within the ±20% mark indicate a high accuracy in estimation, which is also in agreement with the findings by Moradi et al. [19] and Congro et al. [27]. The comparison of the predicted light transmittance and experimental light transmittance within the error range of ±20% is also illustrated in Fig. 15. It can be seen that most of the data points are concentrated along the regression line and within the range of ±20%. This indicates the efficient capability of the trained ANN model in estimating light transmittance of LTC.

6.2. ANN validation

Although R-value, MSE, and RMSE show a good prediction of the trained network, it is necessary to further validate the performance and accuracy of the trained network with new data which has never been exposed to the network. Therefore, a blind test, which is common to be applied in the artificial system [27], was conducted with 10 sets of new data being fed into the trained network to verify the accuracy of the network. The data selected were within the lower limit and upper limit of each variable and parameter.

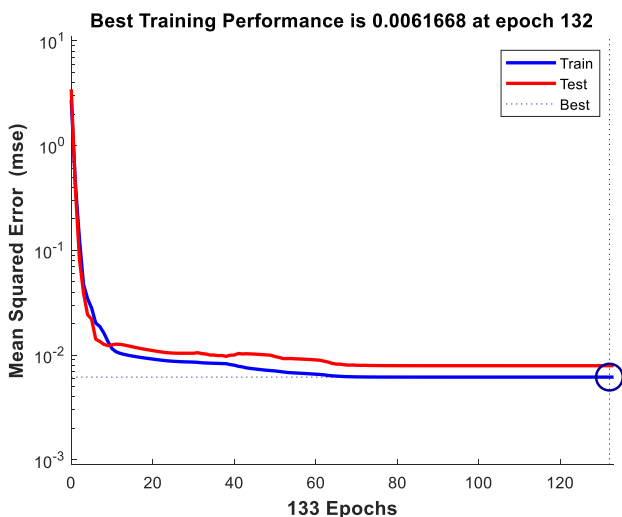Table 6 shows the results of the blind test with the targeted output

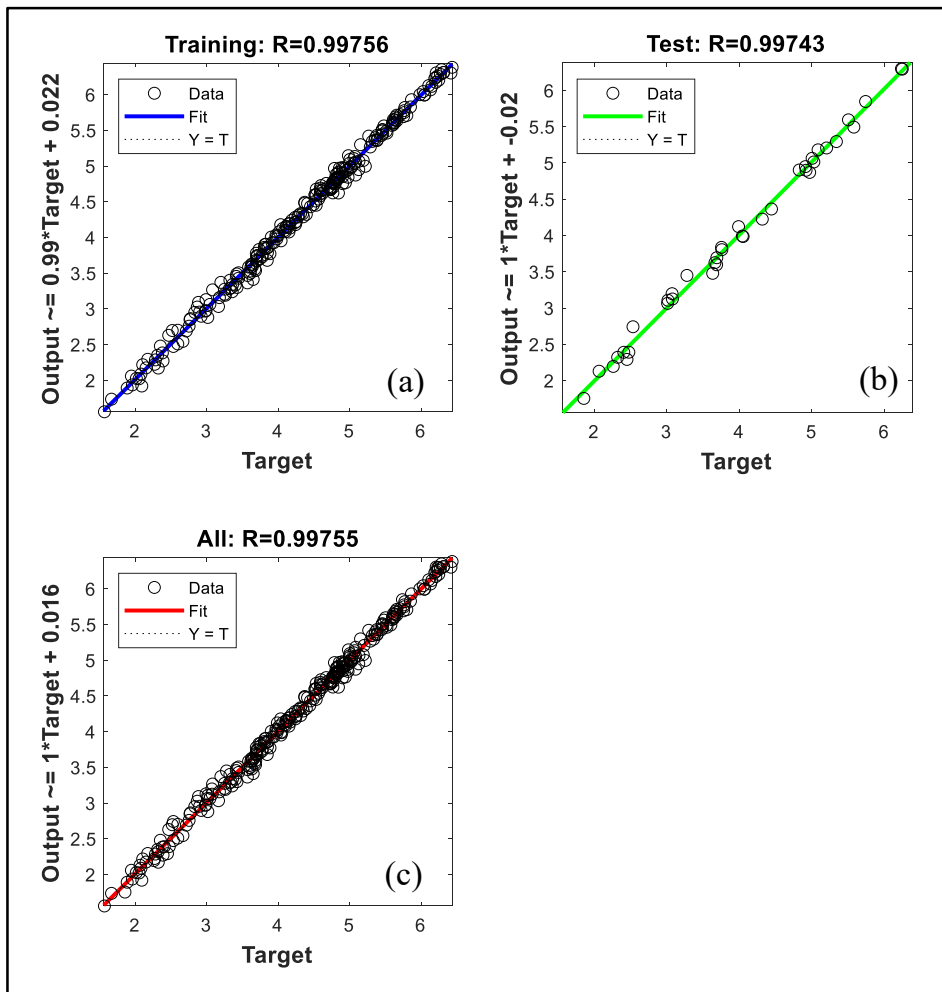**Fig. 11.** The performance of trained ANN model using BR algorithm.

Fig. 12. The correlation between the predicted and targeted output for (a) train data, (b) test data, and (c) all data.
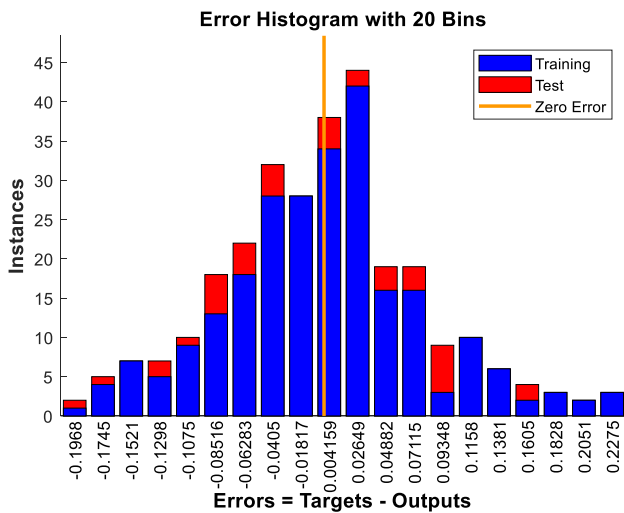

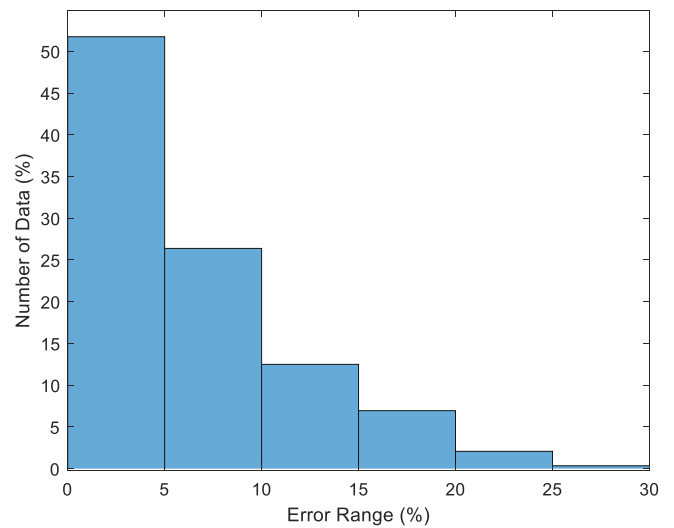**Fig. 13.** Error histogram of the ANN model.

Fig. 14. of estimations in various error ranges.

and predicted output as well as the error of estimation. The scaled values in brackets are the normalised values, which are yet to convert to the actual light transmittance in lux, whereas the values without brackets are the actual light transmittance. It is worth noting that all the estimations are within the 25% error, with the maximum being 23.8% error. Meanwhile, 80% of the estimations are within the 20% error and 70% of them have errors within 15%. The error from the blind test shows consistency with the error range in Figs. 14 and 15, which verifies that the trained ANN model with BR algorithm shows good accuracy in
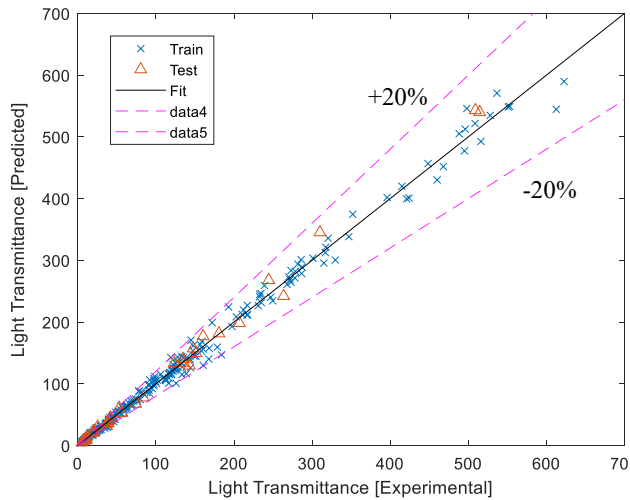
Fig. 15. Comparison of predicted and experimental light transmittance of LTC within the ±20% error.

predicting light transmittance of LTC.

6.3. Explicit equations from trained model

For the convenience of the user, explicit equations were generated from the trained model to predict the light transmittance of LTC. Eq. (9) to Eq. (15) are the net output from the hidden layers according to Eq. (7). After obtaining the net output of H_1 to H_7, they were used in computing the output, O_T based on Eq. (6), where *tansig* and *purelin* transfer functions were also used. Finally, the light transmittance (in unit lux) was obtained through the denormalization of the *mapminmax* function and logarithmic function using Eq. (17) and Eq. (18). However, the input variables must be first normalised using the minimum and maximum values of the respective parameters as stated in Table 4, before using the explicit equations.

$$H_1 = 1.4369 \times \varnothing + 0.0613 \times S - 0.1126 \times n + 1.3478 \times \theta_i + 0.6046 \times L_0 - 0.1428 \tag{9}$$

$$H_2 = 0.9097 \times \varnothing - 0.7222 \times S + 0.0428 \times n - 0.2144 \times \theta_i - 1.007 \times L_0 - 0.6185 \tag{10}$$

$$H_3 = 1.3744 \times \varnothing - 0.2858 \times S + 0.2366 \times n - 0.4101 \times \theta_i - 0.3240 \times L_0 + 1.1475 \tag{11}$$

$$H_4 = 0.6141 \times \varnothing + 0.0929 \times S - 0.1297 \times n + 1.0176 \times \theta_i + 1.1315 \times L_0 - 0.1946 \tag{12}$$

$$H_5 = 0.2401 \times \varnothing + 0.0497 \times S - 0.5555 \times n + 0.4694 \times \theta_i + 0.0386 \times L_0 - 1.0965 \tag{13}$$

$$H_6 = 0.0171 \times \varnothing - 0.1885 \times S - 0.0148 \times n + 1.0686 \times \theta_i - 0.2987 \times L_0 - 0.2061 \tag{14}$$

$$H_7 = 1.8860 \times \varnothing + 0.0837 \times S - 0.1092 \times n + 2.1415 \times \theta_i + 0.6133 \times L_0 + 0.0727 \tag{15}$$

$$O_T = -0.8407 - \frac{3.025}{1 + e^{-2H_1}} + \frac{1.1002}{1 + e^{-2H_2}} + \frac{1.0096}{1 + e^{-2H_3}} + \frac{2.0414}{1 + e^{-2H_4}} - \frac{0.6794}{1 + e^{-2H_5}} - \frac{1.4178}{1 + e^{-2H_6}} + \frac{1.4972}{1 + e^{-2H_7}} \tag{16}$$

$$O_D = \frac{[(O_T + 1)(4.8667)]}{2} + 1.5686 \tag{17}$$

$$L_T = e^{O_D} - 1 \tag{18}$$

where $\varnothing$ is the fibre diameter, S is the fibre spacing, n is the number of blocks, θ_i is the light incidence angle, and L_0 is the initial light intensity.

7. Conclusions

LTC has the potential to transmit natural light to enhance the illuminance in a building and reduce energy consumption for lighting. Therefore, the relationship and effects of variables such as fibre diameter, fibre spacing, surface area, and light incidence angle on the light transmittance of LTC were investigated in this study. Besides that, the obtained experimental results were used to develop an ANN model using the Bayesian Regularization (BR) algorithm, and explicit equations were generated from the trained model. Based on the results obtained from the experimental works and the ANN model developed in this paper, several conclusions can be drawn:

- Light transmittance of LTC increased with a larger fibre diameter and smaller spacing. The light transmittance of LTC increased with a decrease of the solar incidence angle, especially when the solar incidence angle was within the acceptance angle range, namely between 11.00 a.m. and 2.00 p.m. However, the effect of solar

Table 6
Validation analysis using blind test for the ANN model.

Blind test	Input Data					Targeted (Scaled)	Predicted (Scaled)	Error (%) (Scaled)
	$\varnothing$	S	n	θ_i	L_0			
1	2	15	3	12.67	78,000	418.7 (6.0395)	319.2 (5.7690)	23.7582 (4.4791)
2	1.5	15	1	14.99	125,000	276.5 (5.6258)	245.6 (5.5078)	11.1708 (2.0975)
3	2	25	4	29.84	67,600	74.1 (4.3188)	69.9 (4.2615)	5.6461 (1.3272)
4	0.75	15	2	15.52	112,400	60.4 (4.1174)	50.4 (3.9397)	16.5505 (4.3159)
5	2	18.75	6	15.76	83,000	289 (5.6699)	269 (5.5984)	6.9219 (1.2606)
6	2	18.75	4	8.95	100,300	333.3 (5.8120)	327.5 (5.7946)	1.7314 (0.2996)
7	1.5	15	5	0.62	115,100	340.7 (5.8339)	362.3 (5.8952)	6.3368 (1.0502)
8	1.5	15	2	44.96	83,100	41 (3.7377)	35.4 (3.5957)	13.5608 (3.7992)
9	2	25	6	11.49	89,600	182.5 (5.2122)	143.7 (4.9748)	21.2506 (4.5553)
10	0.75	15	1	4.41	117,400	51.6 (3.9627)	47.6 (3.8835)	7.7681 (2.0002)

$\varnothing$: fibre diameter, S: fibre spacing, n: number of blocks, θ_i: light incidence angle, L_0: initial light intensity

incidence angle on light transmittance diminished with smaller fibre diameter and larger fibre spacing.

- The effect of the LTC surface area became significant only with a larger fibre diameter.
- Six blocks arrangement of LTC2.0 with a fibre spacing of 15 mm have the most stable illuminance (no sharp drop) between 12.00 noon and 2.00 p.m. among all the tested blocks.
- The ANN model developed with the Bayesian Regularization (BR) algorithm shows good accuracy in predicting light transmittance of LTC with an MSE of 0.00618 and above 90% of the predicted output being within ±20% of error. This was further validated by a blind test conducted with available experimental data which were never exposed to the network.
- Explicit equations generated from the trained network have a high accuracy in estimating the light transmittance of LTC in a faster and more economical manner.

There are some gaps which are still needed to be bridged in LTC investigation to obtain a comprehensive understanding on LTC before they are implemented in the industry. Some recommendations are suggested in this study:

- It is recommended to have further investigations on the effect of the distance between the specimens and the lux meter, as well as the thermal conductivity of LTC.
- The presence and influence for different sky conditions should be considered in investigating the light transmittance of LTC in the future, to have an insight on the extent of reduction or increment of the amount of light transmitted through LTC.
- Since a larger light area of LTC develops a higher solid angle (especially for different surface areas of wall panels), it is recommended to include the concern of solid angle in future investigation, especially on the effect of surface area towards the light transmittance of LTC wall panels.

- Parameters such as weather conditions, testing location, and light solid angle should be considered in developing an ANN model in future studies, so that the model can be more comprehensive and can be widely used to estimate or determine the performance of light transmittance of LTC.

Credit author statement

Shing Mei Chiew: Conceptualization, Methodology, Resources, Investigation, Writing – Original draft, preparation. **Izni Syahrizal Ibrahim:** Supervision, Writing – Review and editing, Funding acquisition, **Mohd Azreen Mohd Ariffin:** Supervision, **Han-Seung Lee:** Supervision, **Jitendra Kumar Singh:** Supervision.

Declaration of competing interest

The authors declare the following financial interests/personal relationships which may be considered as potential competing interest. Izni Syahrizal bin Ibrahim reports financial support was provided by the Ministry of Higher Education (MoHE) of Malaysia. Shing Mei Chiew, Izni Syahrizal bin Ibrahim, Mohd Azreen bin Mohd Ariffin has patent #IP/CR/04305 licensed to Universiti Teknologi Malaysia.

Data availability

Data will be made available on request.

Appendix

Sample Calculation using explicit equations from ANN model using BR algorithm.

Input Data: $\varnothing = 2$ mm; $S = 15$ mm; $n = 1$; $\theta_i = 59.45°$; $L_0 = 52,100$ lux, Using Eq. (3) to normalise input data, the normalised fibre diameter ($\varnothing_n$) is computed: $\varnothing_n = (2–0.75)/(2–0.75), = 1$.

Similarly

$S_n = 0$; $n_n = 0$; $\theta_{in} = 0.9959$; $L_{0n} = 0.3960$

The normalised input data undergoes the normalisation again using *mapminmax* function (Eq. (8)) built in ANN, where $x_{nmin} = 0$ and $x_{nmax} = 1$. For example,

$$\varnothing_{nn} = 2\frac{(1-0)}{(1-0)} - 1 = 1$$

Similarly, $S_{nn} = -1$; $n_{nn} = -1$; $\theta_{inn} = 0.9919$; $L_{0nn} = -0.2081$.

The normalised data is ready for the explicit expressions.

There are seven neurons in the ANN model developed. The net output of the hidden neurons (H_k) can be computed using Eq. (9) to Eq. (15):

$H_1 = 1.4369 \times \varnothing_{nn} + 0.0613 \times S_{nn} - 0.1126 \times n_{nn} + 1.3478 \times \theta_{inn} + 0.6046 \times L_{0nn} - 0.1428$

$= 1.4369 \times 1 + 0.0613 \times (-1) - 0.1126 \times (-1) + 1.3478 \times 0.9919 + 0.6046 \times (-0.2081) - 0.1428 = 2.5564$

Similarly, $H_2 = 0.9674$; $H_3 = 2.2318$; $H_4 = 1.2301$; $H_5 = 0.1070$; $H_6 = 1.1363$; $H_7 = 3.9806$.

Then, H_k undergoes *tansig* activation function using Eq. (15), given:

$$O_T = -0.8407 - \frac{3.025}{1+e^{-2H_1}} + \frac{1.1002}{1+e^{-2H_2}} + \frac{1.0096}{1+e^{-2H_3}} + \frac{2.0414}{1+e^{-2H_4}} - \frac{0.6794}{1+e^{-2H_5}} - \frac{1.4178}{1+e^{-2H_6}} + \frac{1.4972}{1+e^{-2H_7}}$$

$$= -0.8407 - \frac{3.025}{1+e^{-2(2.5564)}} + \frac{1.1002}{1+e^{-2(0.9674)}} + \frac{1.0096}{1+e^{-2(2.2318)}} + \frac{2.0414}{1+e^{-2(1.2301)}} - \frac{0.6794}{1+e^{-2(0.1070)}} - \frac{1.4178}{1+e^{-2(1.1363)}} + \frac{1.4972}{1+e^{-2(3.9806)}} = -0.1710$$

O_T has to undergo postprocessing from the ANN network using Eq. (16), where $x_{nmin} = 1.5686$ and $x_{nmax} = 6.4365$:

$$-0.1710 = 2 - \frac{(O_D - 1.5686)}{(6.4353 - 1.5686)} - 1$$

$$OD = \frac{(-0.1710 + 1)(4.8667)}{2} + 1.5686 = 3.5858$$

The final prediction of light transmittance (L_T) is computed using Eq. (17)

$$L_T = e^{3.5858} - 1, = 35.0835 \text{ lux}$$

The actual light transmittance is 35.1 lux, for which the absolute relative error $= [|(35.1 - 35.0835)|/35.1] \times 100 = 0.047\%$

References

[1] A. Ahuja, K.M. Mosalam, T.I. Zohdi, An illumination model for translucent concrete using radiance, in: Proc., 14th Conf., Int. Building Performance Simulation Association, 2015, 2586-2579.

[2] X. Su, L. Zhang, Z. Liu, Y. Luo, J. Lian, P. Liang, Daylighting performance simulation and analysis of translucent concrete building envelopes, Renew. Energy 154 (2020) 754–766, https://doi.org/10.1016/j.renene.2020.03.041.

[3] B. Han, L. Zhang, J. Ou, Light-transmitting concrete, in: Smart and Multifunctional Concrete toward Sustainable Infrastructures, Springer, 2017, pp. 273–283.

[4] B. Zhu, Z. Guo, C. Song, Fiber-optic parameters of light emitting diode active-luminous traffic markings based on light-transmitting concrete, J. Tongji Univ. Nat. Sci. 47 (6) (2019) 802–809, https://doi.org/10.11908/j.issn.0253-374x.2019.06.009.

[5] A. Altlomate, F. Alatshan, F. Mashiri, M. Jadan, Experimental study of light-transmitting concrete, International Journal of Sustainable Building Technology and Urban Development 7 (3–4) (2016) 133–139, https://doi.org/10.1080/2093761X.2016.1237396.

[6] S.H. Said, State-of-the-art developments in light transmitting concrete, Mater. Today: Proc. 33 (4) (2020) 1967–1973, https://doi.org/10.1016/j.matpr.2020.06.128.

[7] K. Mosalam, N. Casquero-Modrego, Sunlight permeability of translucent concrete panels as a building envelope, J. Architect. Eng. 24 (3) (2018) 04018015, https://doi.org/10.1061/(ASCE)AE.1943-5568.0000321.

[8] S. Shitote, A. Tuaum, W.O. Oyawa, Experimental evaluation on light transmittance performance of translucent concrete, Int. J. Appl. Eng. Res. 13 (2018) 1209–1218.

[9] S.M. Chiew, I.S. Ibrahim, M.A.M. Ariffin, H.-S. Lee, J.K. Singh, Development and properties of light-transmitting concrete (LTC)–A review, J. Clean. Prod. 284 (2021), 124780, https://doi.org/10.1016/j.jclepro.2020.124780.

[10] B. Huang, Light transmission performance of translucent concrete building envelope, Cogent Engineering 7 (1) (2020), 1756145, https://doi.org/10.1080/23311916.2020.1756145.

[11] A.M. Tahwia, A. Abdel-Raheem, N. Abdel-Aziz, M. Amin, Light transmittance performance of sustainable translucent self-compacting concrete, J. Build. Eng. (2021), 102178, https://doi.org/10.1016/j.jobe.2021.102178.

[12] A.M. Tahwia, N. Abdelaziz, M. Samy, M. Amin, Mechanical and light transmittance properties of high-performance translucent concrete, Case Stud. Constr. Mater. 17 (2022), e01260.

[13] X. Su, L. Zhang, Z. Liu, Y. Luo, P. Liang, J. Lian, An optical and thermal analysis of translucent concrete considering its dynamic transmittance, J. Clean. Prod. (2022), 132588.

[14] F. Lian, Z. Yin, Mechanical, light transmittance properties and simulation study of sustainable translucent lightweight aggregate concrete, Mater. Res. Express 9 (2) (2022), 025507, https://doi.org/10.1088/2053-1591/ac5552.

[15] A. Ahuja, K.M. Mosalam, Evaluating energy consumption saving from translucent concrete building envelope, Energy Build. 153 (2017) 448–460.

[16] A. Ahuja, K.M. Mosalam, T.I. Zohdi, Computational modeling of translucent concrete panels, J. Architect. Eng. 21 (2) (2015). B4014008.

[17] J. Shen, Z. Zhou, "Light transmitting performance and energy-saving of plastic optical fibre transparent concrete products, Indoor Built Environ. (2020) https://doi.org/10.1177/1420326X20903368.

[18] A. Sawant, R. Jugdar, S. Sawant, Light transmitting concrete by using optical fiber, Int. J. Inventive Eng. Sci. 3 (1) (2014) 23–28.

[19] M. Moradi, M. Khaleghi, J. Salimi, V. Farhangi, A. Ramezanianpour, Predicting the compressive strength of concrete containing metakaolin with different properties using ANN, Measurement 183 (2021), 109790.

[20] P.O. Awoyera, Predictive models for determination of compressive and split-tensile strengths of steel slag aggregate concrete, Mater. Res. Innovat. 22 (5) (2018) 287–293.

[21] M.T. Hagan, H.B. Demuth, M. Beale, Neural Network Design, PWS Publishing Co., 1997.

[22] S.R. Mohandes, X. Zhang, A. Mahdiyar, A comprehensive review on the application of artificial neural networks in building energy analysis, Neurocomputing 340 (2019) 55–75.

[23] H. Moayedi, M. Mosallanezhad, A.S.A. Rashid, W.A.W. Jusoh, M.A. Muazu, A systematic review and meta-analysis of artificial neural network application in geotechnical engineering: theory and applications, Neural Comput. Appl. 32 (2) (2020) 495–518.

[24] K. Ramkumar, P.K. Rajkumar, S.N. Ahmmad, M. Jegan, A review on performance of self-compacting concrete–use of mineral admixtures and steel fibres with artificial neural network application, Construct. Build. Mater. 261 (2020), 120215.

[25] T. Gupta, K. Patel, S. Siddique, R.K. Sharma, S. Chaudhary, Prediction of mechanical properties of rubberised concrete exposed to elevated temperature using ANN, Measurement 147 (2019), 106870.

[26] S. Chithra, S.S. Kumar, K. Chinnaraju, F.A. Ashmita, A comparative study on the compressive strength prediction models for High Performance Concrete containing nano silica and copper slag using regression analysis and Artificial Neural Networks, Construct. Build. Mater. 114 (2016) 528–535.

[27] M. Congro, V.M. de Alencar Monteiro, A.L. Brandão, B.F. dos Santos, D. Roehl, F. de Andrade Silva, Prediction of the residual flexural strength of fiber reinforced concrete using artificial neural networks, Construct. Build. Mater. 303 (2021), 124502.

[28] D. Merchant, P. Scully, N. Schmitt, Chemical tapering of polymer optical fibre, Sensor Actuator Phys. 76 (1–3) (1999) 365–371, https://doi.org/10.1016/S0924-4247(99)00008-4.

[29] T.d.S. Henriques, D.C. Dal Molin, Â.B. Masuero, Optical fibers in cementitious composites (LTCM): analysis and discussion of their influence when randomly arranged, Construct. Build. Mater. 244 (2020), 118406, https://doi.org/10.1016/j.conbuildmat.2020.118406.

[30] Y. Li, J. Li, H. Guo, Preparation and study of light transmitting properties of sulfoaluminate cement-based materials, Mater. Des. 83 (2015) 185–192, https://doi.org/10.1016/j.matdes.2015.06.021.

[31] D. Navabi, M. Javidruzi, M.R. Hafezi, A. Mosavi, The high-performance light transmitting concrete and experimental analysis of using polymethylmethacrylate optical fibers in it, J. Build. Eng. 38 (2021), 102076, https://doi.org/10.1016/j.jobe.2020.102076.

[32] R. Siddique, Properties of self-compacting concrete containing class F fly ash, Mater. Des. 32 (3) (2011) 1501–1507, https://doi.org/10.1016/j.matdes.2010.08.043.

[33] P. Dinakar, M.K. Reddy, M. Sharma, Behaviour of self compacting concrete using Portland pozzolana cement with different levels of fly ash, Mater. Des. 46 (2013) 609–616, https://doi.org/10.1016/j.matdes.2012.11.015.

[34] N. Miura, N. Takeda, R. Chikamatsu, S. Sogo, Application of Super Workable Concrete to Reinforced Concreted Structures with Difficult Construction Conditions, vol. 140, Special Publication, 1993, pp. 163–186.

[35] L.S. Ho, T.-P. Huynh, Long-term mechanical properties and durability of high-strength concrete containing high-volume local fly ash as a partial cement substitution, Results in Engineering 18 (2023), 101113.

[36] Admixtures for Concrete, Mortar and Grout. Concrete Admixtures-Definitions, Requirements, Conformity, Marking and Labeling, B. S. Institution, 2012.

[37] M. B. Solutions, "MasterGlenium® ACE 8589." Master Builders Solutions. https://assets.construction-chemicals.mbcc-group.com/en-my/masterglenium%20ace%208589.pdf.

[38] The European Guidelines for Self-Compacting Concrete: Specification, Production and Use, T. E. F. o. S. C. C. a. C. Systems, 2005.

[39] Testing Hardened Concrete: Compressive Strength of Test Specimens, B. S. Institution, 2009.

[40] MS 2680, Energy Efficiency and Use of Renewable Energy for Residential Buildings - Code of Practice, M. Standard, 2017, 2017.

[41] L CASIO COMPUTER CO., Solar elevation angle (for a day) Calculator. https://keisan.casio.com/exec/system/1224682277, 2021.

[42] S.A. Ziaee, E. Sadrossadat, A.H. Alavi, D. Mohammadzadeh Shadmehri, Explicit formulation of bearing capacity of shallow foundations on rock masses using artificial neural networks: application and supplementary studies, Environ. Earth Sci. 73 (7) (2015) 3417–3431.

[43] Y. Liu, L. Ji, R. Huang, T. Ming, C. Gao, J. Zhang, An attention-gated convolutional neural network for sentence classification, Intell. Data Anal. 23 (5) (2019) 1091–1107.

[44] D.R. Baughman, Y.A. Liu, Fundamental and practical aspects of neural computing, in: Neural Networks in Bioprocessing and Chemical Engineering, Elsevier, 1995, pp. 21–109.

[45] H. Garoosiha, J. Ahmadi, H. Bayat, The assessment of Levenberg–Marquardt and Bayesian Framework training algorithm for prediction of concrete shrinkage by the artificial neural network, Cogent Engineering 6 (1) (2019), 1609179.

[46] A. Clayton. "Why are temperatures warmer at the Equator? " WKBN First News 27. https://www.wkbn.com/weather/why-are-temperatures-warmer-at-the-equator/.